Digital Object Identifier (DOI): 10.1109/APEC.2016.7468209

IEEE Transactions on Power Electronics

Quadruple Active Bridge DC-DC converter as the basic cell of a modular Smart Transformer

Levy Ferreira Costa
Giampaolo Buticchi
Marco Liserre

Quadruple Active Bridge DC-DC Converter as the Basic Cell of a Modular Smart Transformer

Levy F. Costa, Giampaolo Buticchi and Marco Liserre, *Fellow*, IEEE
Christian-Albrecht-University of Kiel (Uni-Kiel) / Power Electronics Chair (PE)
Kaiserstr. 2, 24143, Kiel, SH, Germany
Email: {lfc, gibu, ml}@tf-uni-kiel.de

***Abstract*—One of the main challenges of a Solid-State transformer (SST) lies in the dc-dc conversion stage. In this work, a Quadruple-Active-Bridge (QAB) dc-dc converter is investigated to be used as the basic module for the whole dc-dc stage. Besides the feature of high power density and soft-switching operation, the QAB converter provides a solution with a reduced number of high frequency transformers, since more bridges are connected to the same multi-winding transformer. To ensure soft-switching in the full operation range of the converter, two modulation strategies are investigated: the phase-shift modulation and the triangular current modulation. The theoretical analysis is developed for both modulation strategies and a comparison between them is carried out. In order to validate the theoretical analysis, a 20 kW prototype was built and tested.**

I. Introduction

In recent years, the smart grid technologies have received more and more attention, as a feasible solution to manage in an efficient way the increased demand and the high penetration of distributed generation (DG). One of these technologies is the Smart Transformer, which is a Solid-State Transformer [1] - [2] with control and communication functionality [3]. This power electronics based system uses a high frequency (HF) transformer, reducing volume and weight, and it can also provide ancillary services to the grid, such as: power factor correction, active filtering, VAR compensation, electronics protection and disturbance rejection [1] - [2].

The three-stage ST is usually composed of a Medium-Voltage (MV) ac-dc stage, a HF isolated dc-dc stage and a Low-Voltage (LV) dc-ac stage. The main challenge of this architecture is the dc-dc conversion stage, since it has strict requirements, such as: high rated power, high current capability in LV side, high voltage capability in HV side, high frequency isolation and high efficiency.

To meet all these requirements, two solutions have been widely investigated: the first one is to use standard converter with high voltage rating devices [4] - [5], while the second one is based on the modular concept, in which several modules are used to share the total voltage and power among them [6] - [8]. Although the modular solution presents a high component count, it has several advantages compared to the fist solution, such as: low dv/dt (low EMI emission), possibility to use standard low voltage rating devices and also modularity, which enables fault tolerance capability.

Several converters have been investigated to be used as module of the main core of the ST, but the Dual-Active-Bridge (DAB) and the Series-Resonant converter (SR) have received more attention, due their advantages of soft-switching, high efficiency and power density [9] - [8]. The Series-Resonant dc-dc converter presents a well regulated output voltage for wide range of load (when operating in discontinuous-conduction-mode), avoiding the requirement of control loops. For that reason, it is also called dc-transformer [6] - [8]. On the other hand, when the output voltage control or power flow control is required, the DAB converter is more advantageous, since it enables the active control of the transferred power [9] - [11].

The Multiple Active Bridge (MAB) is an alternative solution for the DAB or SRC. This kind of converter was firstly introduced in [12] and it was applied in a solid-state transformer in [13], in order to connect renewable energy

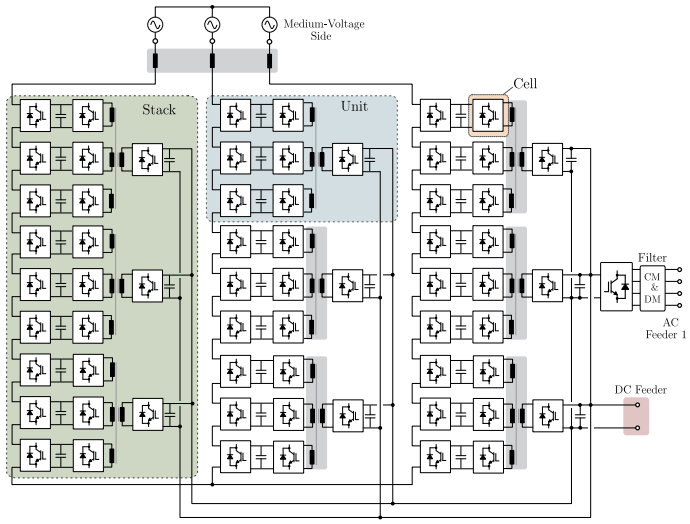

Fig. 1. Modular smart transformer architecture using the QAB converter as a basic module of the dc-dc conversion stage.

TABLE I
Specification of a Smart Transformer for distribution system

Specification	Smart Transformer	Specification	QAB
Rated Power	1 MVA	Rated Power	111 kW
Input Voltage	400 V	Input voltage (LV)	700 V
Output Voltage	10 kV	Output voltage (MV)	1.13 kV
LVDC link	700 V	Switching frequency	20 kHz
MVDC link	10.2 kV	IGBT	1700 V

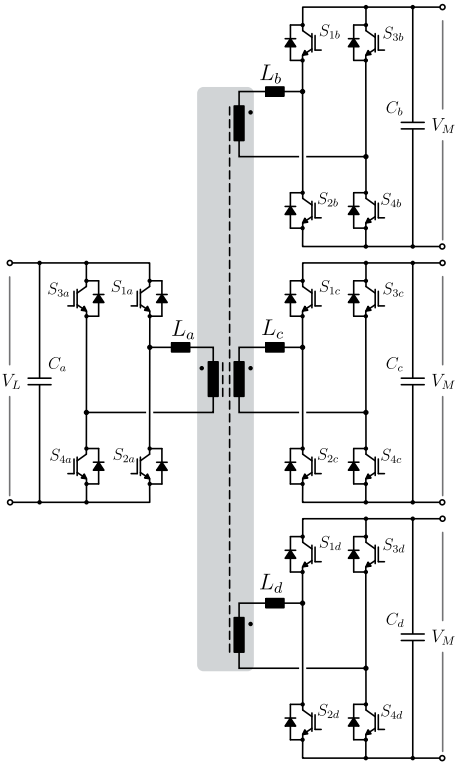

Fig. 2. Topology of the Quad-Active-Bridge dc-dc converter.

sources and storage system to the grid. The MAB converter has the same features of the DAB converter, with the additional characteristic to reduce the number of the HF transformers, since the MAB converter integrates more active bridges into a single transformer. In this context, this paper investigates the application of the Quad-Active-Bridge (QAB) dc-dc converter as a basic converter to build the entire ST system.

The QAB converter is composed of four active bridges connected to the same HF transformer. Fig. 1 shows the ST architecture using the QAB converter as a basic module of the dc-dc stage, while Fig. 2 shows the topology of the QAB converter. A basic specification of the QAB converter for distribution system application is presented in Table I, where a very high Medium Voltage DC (MVDC) link is required. In order to share the MVDC link with the maximum number of modules, three bridges of the QAB converter are connected to the MV side, while only one is connected in the LV side, as illustrated in Fig. 1. Table I lists the specification of the QAB converter.

The main contribution of this paper is the investigation of the QAB converter as a basic cell for a modular ST application. To control the converter, the well-known phase-shift modulation is initially considered. Nevertheless, this modulation method has some limitations regarding the soft-switching operating range, when the output voltage varies. For this reason, an alternative scheme based on the triangular current modulation is also investigated in this paper. In section II, the operation principle of the converter is presented and both modulations schemes are described. The semiconductors

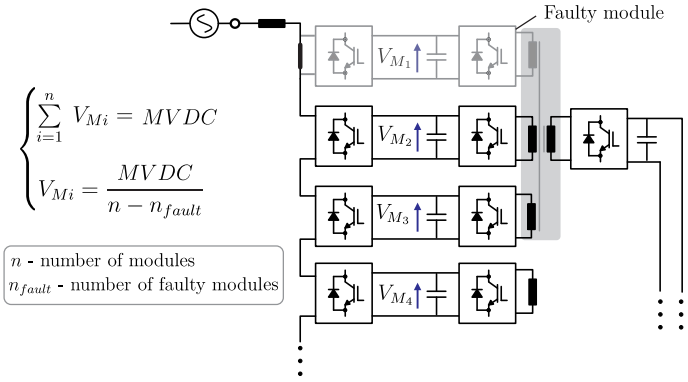

Fig. 3. Simplified diagram of the ST, illustrating the fault operation of the system, with one faulty cell.

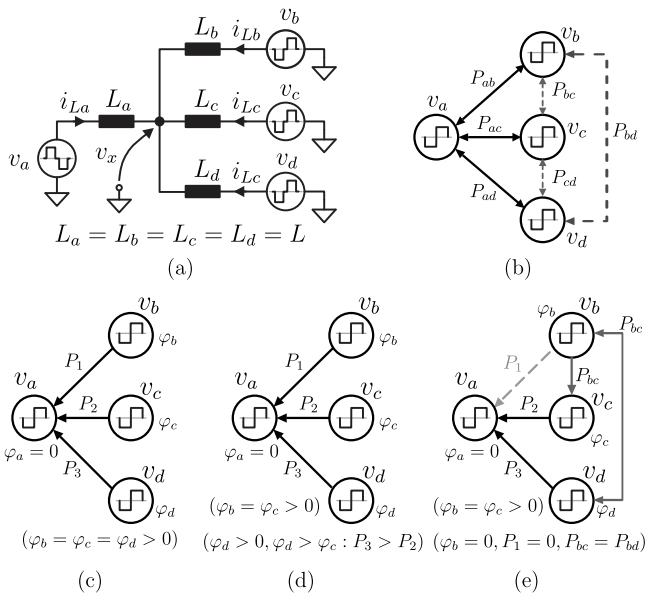

Fig. 4. Equivalent circuit of the QAB converter and possible power transfer path among the actives bridges: (a) Equivalent circuit. (b) All possible power path of the converter. (c) Normal balanced condition case, where the LV cell a receives equal power from the three MV cells (b, c and d), (load: cell a, sources: cell b, c and d). (d) Unbalanced condition case, where the LV cell a receives different power from the MV cells (b, c and d), and in this example the cell d delivers more power than the cells b and c; (load: cell a, source: cell b, c and d). (e) Unusual case, where the MV cell b operates as a source, giving energy to cells (b and c), (load: cell a, sources: cell b, c and d). In the last case, $P_1 = 0$.

current effort and transformer current effort are presented and discussed in Section III. In section IV, the operation of the QAB converter with unbalanced load in the MV cells and the impact on the structure is discussed. Finally, experimental results obtained for both modulation strategies under investigation are presented in Section V.

II. Operation Principle

The QAB is composed of four active bridges and for the analysis, each of them is denoted by the letters a, b, c and d. The elements of the bridges have sub-index $i = \{a, b, c, d\}$ to indicate the bridge the element belongs to, as depicted in Fig. 2. In ST application, the bridge a is connected to the LV side,

while the bridges b, c and d are connected to the MV side. All bridges can exchange power among themselves and the possible power paths are depicted in Fig. 4 (b), where each bridge is symbolized by the voltage source v_i.

In standard operation, the power flows from the MV to the LV side and the bridges b, c and d process the same amount of power, i.e. balanced power condition, given by P_1, P_2 and P_3, respectively. This point of operation is represented in Fig. 4 (c).

The unbalanced condition, where the powers P_1, P_2 and P_3 are positive, but not equal, is also a common operation in ST application and this situation is depicted in Fig. 4 (d). This condition can happen in case of a dynamic response of the system, where the MV cells process unbalanced instantaneous power or even intentionally to perform other kinds of optimization.

An unusual operation is depicted in Fig. 4 (e), where the power flows not only from the MV to the LV side, but also from one MV cell to the others MV cells. In this situation, a MV cell operates as source and load. Although this situation is very unlikely, it is presented here to demonstrate the versatility of the QAB converter in ST application.

Similarly to the DAB, there are several possibilities to modulate the QAB converter. Originally, the classical phase-shift modulation strategy has been applied to most multiple active bridge solutions present in literature.

Nevertheless, a different modulation strategy based on the Triangular Current Modulation (TCM) was applied to the QAB converter in [14], as a possible solution to increase the soft-switching range in variable output voltage conditions. In standard operation of the ST, variation on the QAB converter output voltage is not expected. However, in fault case one or more faulty cells are disconnected from the system, as depicted in Fig. 3, and then all the remaining cells must reconfigure the system adjusting its output voltage, in order to keep the MVDC link in the correct value after the fault. For this condition, the PSM might operate with hard switching and this motivates the investigation of the TCM for QAB converter. In this paper these two modulation strategies will be compared.

To analyze the converter, an equivalent circuit based on the Y-model and depicted in Fig. 4 (a) is used, in which the bridges are replaced by rectangular voltage sources (v_a, v_b, v_c and v_d). The voltage on the central point v_x and the current slope of each inductor are given by (1) and (2), respectively, where $k = \{a, b, c, d\}$.

$$v_x = \frac{v_a + v_b + v_c + v_d}{4} \tag{1}$$

$$\frac{di_{Lk}}{dt} = \frac{(v_k - v_x)}{L} \tag{2}$$

A. Phase-Shift Modulation Strategy

For phase-shift operation, rectangular voltages v_a, v_b, v_c and v_d with phase shift φ_a, φ_b, φ_c and φ_d, respectively, and constant switching frequency f_s are applied to the transformer. The power is controlled by the phase difference among the bridges and it can be generally described as

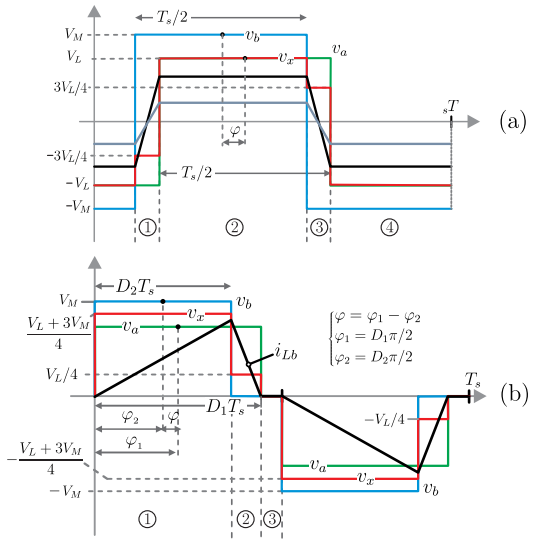

Fig. 5. Main waveforms of the QAB converter, considering positive power flow (from the MV to the LV side): (a) PSM, (b) TCM.

$$P_{ik} = \frac{V_M V_L}{2\pi f_s L n}\varphi_{ik}\left(1 - \frac{|\varphi_{ik}|}{\pi}\right), \ \varphi_{ik} = \varphi_i - \varphi_k \tag{3}$$

where, $i = a, b, c, d$ and $k = a, b, c, d$, according to [13]. In this work, the LV bridge is used as the reference cell, thus it is defined that $\varphi_a = 0$. In the case, the power exchanged among the cells a and b is given by (4). The main waveform of the PSM is shown in Fig. 5 (a).

$$P_1 = \frac{V_M V_L}{2\pi f_s L n}\varphi_b\left(1 - \frac{|\varphi_b|}{\pi}\right) \tag{4}$$

The PSM is characterized by ZVS turn-on, but this features depends on the input and output voltages relation and also the load [15]. As the input and output voltage are considered constant, the converter can be properly designed to work with ZVS operation for its entire range of operation. As a disadvantage, a high level of reactive power that circulates in the high frequency transformer when the phase-shift operation angle is high. Therefore, to avoid high reactive circulating current, a relatively low nominal phase-shift angle must be chosen on the converters design.

B. Triangular Current Modulation Strategy

The TCM was previously applied to the DAB converter in [16] and then extended to the QAB converter in [14]. Differently from the previous modulation strategy, the TCM uses the duty-cycle to control the power transferred among the bridges. Using the TCM, the switches of the MV cells can operate with ZCS and the circulating reactive power on the converter can be reduced. However, the current on the semiconductors and transformer can have a high root-mean-square (rms) value, due to the triangular current shape with high peak, impacting on the conduction losses.

In this analysis, it is considered that the QAB converter operates in balanced condition, i.e. $P_1 = P_2 = P_3$ and the LV

bridge duty-cycle is given by D_1, while the voltage of the MV cells b, c and d are given by D_2, D_3 and D_4, respectively. As the balanced condition is considered, then $D_2 = D_3 = D_4$.

The basic principle of the TCM is to impose a triangular current on the inductors, as shown in Fig. 5 (b). To achieve that, the voltages v_a and v_b should have the waveforms depicted in Fig. 5 (b) and consequently the voltage v_x is

$$v_x = \begin{cases} \dfrac{nV_L + 3V_M}{4}, & 0 < t < d_2 T_s \\ \dfrac{nV_L}{4}, & d_2 T_s < t < d_1 T_s \\ 0, & d_1 T_s < t < T_s/2 \end{cases} . \tag{5}$$

As can seen in Fig. 5 (b), the current in the inductor starts from zero and reaches its maximum value Δi_{Lb} during the period of time between $0 < t < D_2 T_s$, where T_s is the switching period.

The current variation during this period, denoted as $\Delta i_{Lb_{(0<t<D2Ts)}}$, can be calculated by using (2), where v_x is given by (5). As the currents start from zero, the switches S_2 and S_3 of the LV side and also the switches S_5 and S_6 of the MV side turn-on at Zero-Current-Switching (ZCS).

Likewise, during the period $0 < t < D_2 T_s$, the currents decrease from Δi_{Lb} until reaches zero again. For this period, the current variation denoted as $\Delta i_{Lb_{(D2Ts<t<Ts)}}$ can also be calculated by (2). In the moment $t = D_2 T_s$, the current is zero and the switch S1 turned-off at ZCS.

To achieve ZCS operation regardless the load and input or output voltages levels, the condition $\Delta i_{Lb_{(0<t<D2Ts)}} = \Delta i_{Lb_{(D2Ts<t<Ts)}}$ must be satisfied. As a results, the relation between the duty-cycle D_1 and D_2 is found and presented in (6).

The total power transferred from the LV to the MV is given by (7) [14]. Thus, the duty-cycle of the LV bridge D_1 can be used to control the power transferred from the MV to the LV side, while the duty-cycle of the MV bridges, $D_{2,3,4}$ can be calculated to ensure the ZCS operation of the converter.

$$D_2 = \frac{V_L \cdot n}{V_M} D_1 \tag{6}$$

$$P_{(tot)} = \frac{3{D_1}^2 (V_L n)(V_M - V_L n)}{4 L f_s} \tag{7}$$

III. Semiconductors and Transformer Effort

In order to evaluate the performance in terms of efficiency of the QAB converter with both modulation strategies, the current effort on the semiconductors and transformer, as well as the power losses in these elements are calculated and compared.

For the PSM, the current waveforms on the primary side transformer and also on the semiconductors of the LV bridge and MV bridge are depicted in Fig. 6. To calculate the rms and average value of these waveforms, the equations (8) and (9) are used. Similarly, for the TCM, the current waveforms are shown in Fig. 6. The current efforts on the semiconductors and

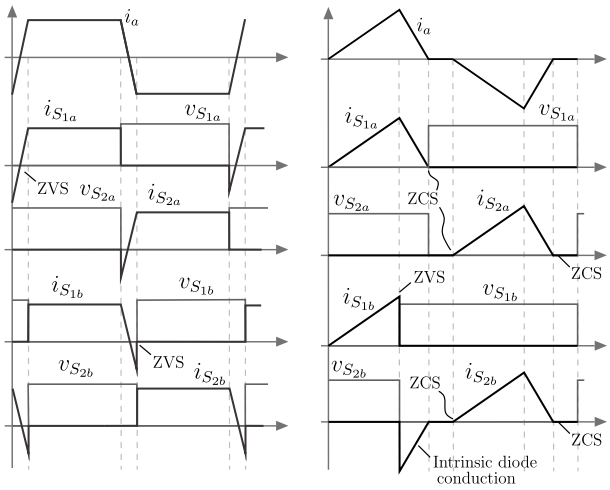

(a) PSM (b) TCM

Fig. 6. Current waveform on the semiconductors and transformer of the QAB converter, for both analyzed modulation schemes.

transformer for this modulation method were demonstrated in [14] and the equations are used in this work. The efforts are calculated taking into account the specification shown in Table I and the results are presented in Fig. 7. To evaluate the performance of the converter for the entire possible range of operation, a maximum phase shift of $\varphi = 90°$ for the PSM and a maximum duty-cycle of $D = 0.5$ for the TCM were considered. The inductor was designed in order to have the maximum power at maximum control variable (phase angle for the PSM and duty-cycle for the TCM), resulting a $L = 80\mu H$ for PSM and $L = 22.5\mu H$ for TCM.

$$i_{S1a,rms} = \sqrt{\frac{1}{T_s} \int_0^{T_s} {i_{S1a}}^2 (t)\, dt} \tag{8}$$

$$i_{La,avg} = \frac{1}{T_s} \int_0^{T_s} i_{La}(t)\, dt \tag{9}$$

As can be seen in Fig. 7 (a), the rms current in the semiconductor of the MV cell are always lower for the PSM, compared to the TCM. However, for the primary side current, there is a region where the TCM presents lower rms current. The main reason for that is the high reactive power on the converter due to the high phase shift operation angle. This effect is also observed in the rms current on the transformer primary side, depicted in Fig. 7 (c).

The average current through the semiconductors for both modulation methods are shown in Fig. 7 (b). According to this graphic, the primary side semiconductors carry the same average current for both modulation methods. However, the average current on the secondary side semiconductors are higher for the TCM method. Therefore, for this graphics, higher conduction losses for the TCM compared to the PSM are expected.

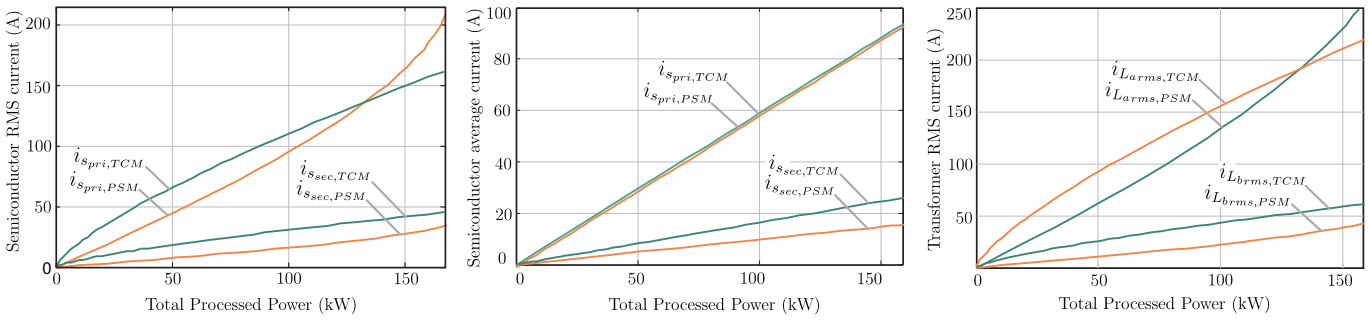

Fig. 7. Current effort on the semiconductor and transformer as function of the total transferred power for both modulation methods and considering balanced condition: (a) rms current on the semiconductors, (b) average current on the semiconductors, (d) rms current on the transformer primary side.

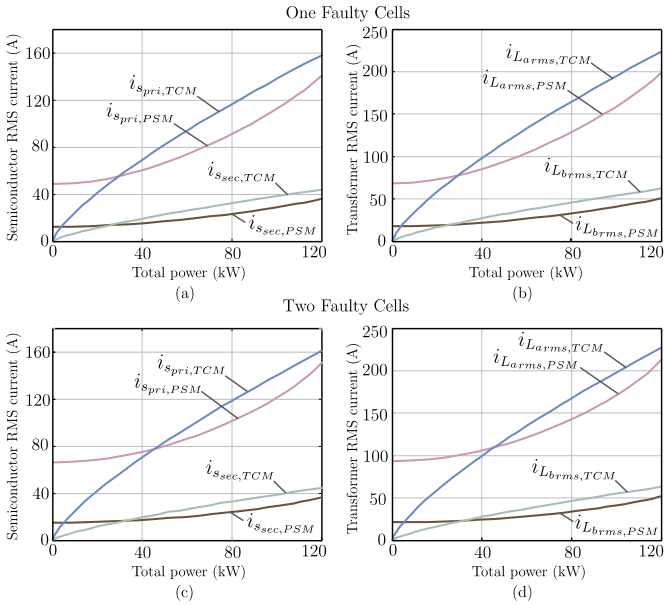

Fig. 8. Current effort on the semiconductor and transformer for fault case.

In a fault case, the output voltage of the remaining QAB converter cells must be adjusted in order to compensate the faulty cell, providing a regulated MVDC link after the fault. The variation of the QAB converter output voltage has impact on the current efforts of the semiconductors and transformer. Fig. 8 shows the current effort on the semiconductor and transformer, in case of a fault of one and two cells. As can be noticed, the current efforts increase significantly for low power (lower than 25% of the total power) when the QAB operates with the PSM and one faulty cell. In case of two faulty cells and PSM operation, the current efforts is even higher for processed power lower than 43% of the total power. Thus, in faulty operation, it is more advantageous to employ the TCM in case of light load. Moreover, in this condition the ZVS operation achieved with the PSM is not ensured anymore, and switching losses will be added in the converter losses.

IV. Unbalanced Condition

In the theoretical analysis performed so far, steady-state and balanced condition is considered, i.e. $P_1 = P_2 = P_3$. Nevertheless, situation in which different power level are processed by the MV cells will happen often in ST. For that reason, the performance of the converter during unbalanced condition is also studied in this work.

Fig. 9 shows the main voltage and current waveforms of the QAB converter for unbalanced condition. Regardless the modulation strategy, the inductor current waveform might have a high rms value in highly unbalanced operation, as those cases presented in [13] and [12]. However, for ST application, it is considered that the power flowing in each bridge does not change its direction, but only the power level is changed, as the case presented in Fig. 4 (c). Thus, the MV currents (i_{Lb}, i_{Lc} and i_{Ld}) waveforms will be modified, but the impact on the i_{La} current is minimum.

For the PSM, the main waveforms are shown in Fig. 9 (a) for a realistic situation in unbalanced condition, in which one MV cell processes around 30% more power than the other MV cells. The imbalance can be easily observed on the current waveforms i_{Lb} and i_{Lc}, but slightly noticed on the current i_{La}. This represents a great advantage of this structure, since an imbalance does not affect significantly the LV cell, which is responsible for the major losses of the converter, due to its high current. Fig. 10 (a) shows the current effort on the semiconductors of the cells b and c, when the QAB converter operates with PSM and an imbalance of 15% (i.e. one MV cell c process 15% more power then the others) and 30%. This graphic was plotted using the same specifications and parameters already presented in Section III.

For the TCM scheme, the main waveforms are shown in 9 (b) for a condition where the bridge c procesess 30% more power than the others bridges. In this case, the duty-cycle D_3 of the cell c is slightly higher than the D_2 and D_4. It is important to note in this figure that the imbalance causes the loss of the ZCS, adding switching losses to the converter, since the current starts from a small constant dc value, but different from zero.

As can be observed in Fig. 9 (b), the voltage v_x has one more level, caused by the duty-cycle difference given by $\Delta D = D_3 - D_2$, and this additional level makes the current i_b decrease and the current i_c increase. Afterward, both currents decrease with the same slope, but they reach different values, because they started from different points. As a conclusion, the

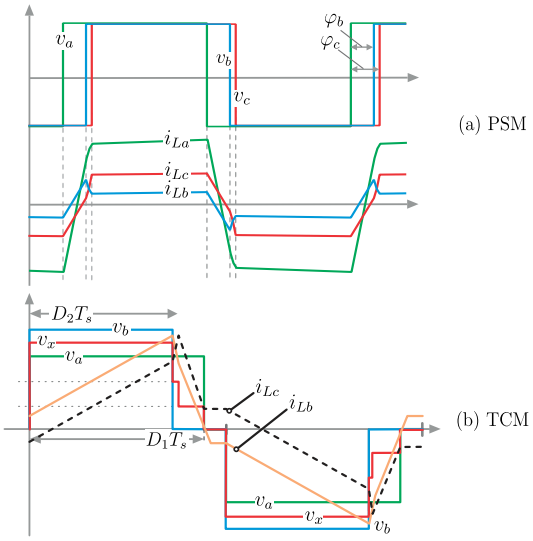

Fig. 9. Main current and voltage waveforms of the QAB converter for unbalanced condition.

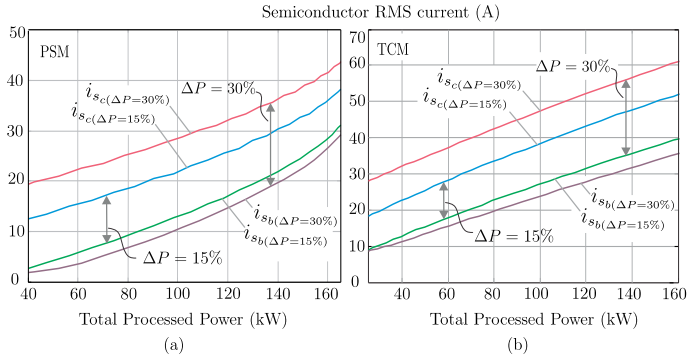

Fig. 10. Semiconductors effort of the QAB converter for an imbalance of 15% and 30%.

variable ΔD has direct impact on the dc value of the currents, and consequently the additional power delivered by the MV cell. For that reason, this new variable can be used to control the power exchange among the MV cells, as described in [14].

Fig. 10 (a) shows the current effort on the semiconductors of the cells b and c, when the QAB converter operates with TCM and an imbalance of 15% (i.e. one MV cell processing 15% more power then the others) and 30%, in order to point out the imbalance on the semiconductors effort.

V. Experimental Results

In order to verify the operation and evaluate the performance of the QAB converter with both modulation strategies, a 20 kW prototype was designed, and the converter performance was verified experimentally.

The converter specifications, as well as the selected components used in the prototype are shown in Table II.

As can be noticed in Section III, the required inductance for the TCM is lower than the value required for the TCM. Likewise, for the PSM the transformer turn ratio should be chosen in order to have the same voltage level on the primary side and reflected secondary side. However, this situation must be avoided for the TCM. As the experimental results were obtained for both modulation methods using the same prototype, different output voltages were utilized, according to the modulation strategy, in order to have similar performance.

The experimental results consist of the relevant voltage and current waveforms for steady-state operation of the QAB converter using both presented modulation methods. The main waveforms obtained from the prototype are shown in Fig. 11. Considering the limitations of dc voltage sources, the LV port was connected to the DC supply and the ohter ports were connected to loads (reverse power flow operation).

The results of the converter operating with TCM for balanced and unbalanced loads are shown in Fig. 11 (a) and (b), respectively. In Fig. 11 (a), the converter processes around 2.2 kW, divided equally among the MV cells. As expected, the current and voltage waveforms are very similar to the theoretical waveforms and the ZCS feature can be noticed in the figure. Fig. 11 (b) shows the results for unbalanced condition, where the bridges b and d process 640 W, while the bridge c process 480 W, resulting in a total power of approximately 1.8 kW. For safety reasons (open semiconductor modules without the insulating gel), the test was performed with voltage of 150V in the secondary side. As can seen in Fig. 11 (b), the ZCS feature is lost.

Similarly, Fig. 11 (c) and (d) show the results for the QAB converter operating with PSM. It is important to note that the PSM modulation results were obtained with switching frequency of 40 kHz.To ensure ZVS operation, the results were obtained for the same input and output voltage of 200 V. The results for balanced load condition is depicted in Fig. 11 (c) and it is presented just to point out the proper operation of the QAB converter. In Fig. 11 (c), the imbalance can be noticed on the waveform of the current i_{Lb}. However, this effect is not very evident on the current i_{La}.

VI. Conclusion

In the framework of Solid-State transformer development, modular architectures will play a fundamental role. In this paper, a quadruple active bridge converter is employed as a basic cell of the dc-dc conversion stage of the ST. The theoretical analysis of the QAB converter was carried out considering the phase-shift modulation scheme and the triangular current modulation. From the comparison it is observed that in standard operation the phase-shift modulation presents lower current effort on the semiconductors and transformer, compared to the triangular current modulation, implying also reduced conduction losses. However, in a fault case, where the system must be reconfigured and the MV cells must work with higher voltage, the triangular current modulation is more advantageous.

Moreover, the theoretical analysis and experimental results showed that unbalanced load in the MV cells has an insignificant effect on the primary side current, which is responsible for the major converter losses. In other words,

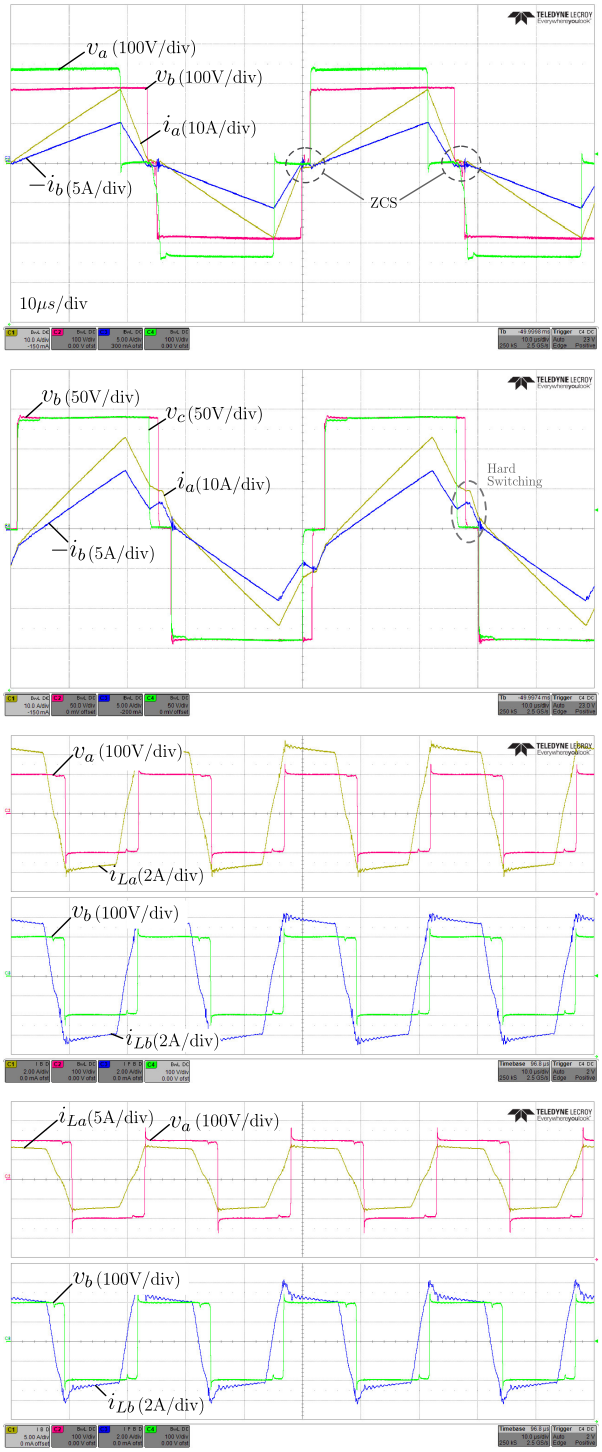

Fig. 11. Experimental results of the QAB converter using both modulation strategies and considering balanced and unbalanced conditions: (a) for the TCM and balanced load condition, (b) for the TCM and imbalance of 25%, (c) for the PSM and balanced load condition, (d) for the PSM and imbalance on the MV side.

TABLE II
SPECIFICATION OF THE QAB DC-DC CONVERTER PROTOTYPE

Parameter	Value
Rated Output Power	$P_o = 20kW$
LV dc-link (V_a)	$V = 200V$
MV dc-link (V_b, V_c, V_d)	$V = 250V$
Switching frequency	$f_s = 20kHz$
Leakage inductance	$L_a = L_b = L_c = L_d = 35\mu H$
Transformer turn ratio	$n = 1:1:1:1$
Output filter capacitor	$C = 500\mu F$
IGBT $S_{1,2,3,4}$	Infineon SIGC32T120R3E IGBT3 (1200V/25A)

for the configuration used in this work, the current effort on the primary side and consequently the conduction losses is unaffected by the imbalance in the MV cells.

REFERENCES

[1] X. She, R. Burgos, G. Wang, F. Wang, and A. Huang, "Review of solid state transformer in the distribution system: From components to field application," in *IEEE Energy Conversion Congress and Exposition (ECCE)*, Sept 2012, pp. 4077–4084.

[2] J. W. Kolar and G. Ortiz, "Solid-state-transformers: Key components of future traction and smart grid systems," in *Proceedings of the International Power Electronics Conference - ECCE Asia (IPEC 2014)*, May 2014.

[3] G. De Carne, M. Liserre, K. Christakou, and M. Paolone, "Integrated voltage control and line congestion management in active distribution networks by means of smart transformers," in *IEEE 23rd International Symposium on Industrial Electronics (ISIE)*, June 2014, pp. 2613–2619.

[4] R. W. D. D. N. Soltau, R. U. Lenke, "High-power dc-dc converter," Technical Report, Rheinisch-Westflische Technische Hochschule, 2013.

[5] D. Rothmund, J. Huber, and J. Kolar, "Operating behavior and design of the half-cycle discontinuous-conduction-mode series-resonant-converter with small dc link capacitors," in *Control and Modeling for Power Electronics (COMPEL), 2013 IEEE 14th Workshop on*, June 2013, pp. 1–9.

[6] D. Dujic, G. Steinke, E. Bianda, S. Lewdeni-Schmid, C. Zhao, and J. Steinke, "Characterization of a 6.5kv igbt for medium-voltage high-power resonant dc-dc converter," in *Applied Power Electronics Conference and Exposition (APEC), 2013 Twenty-Eighth Annual IEEE*, March 2013, pp. 1438–1444.

[7] D. Dujic, A. Mester, T. Chaudhuri, A. Coccia, F. Canales, and J. Steinke, "Laboratory scale prototype of a power electronic transformer for traction applications," in *Power Electronics and Applications (EPE 2011), Proceedings of the 2011-14th European Conference on*, Aug 2011, pp. 1–10.

[8] C. Zhao, D. Dujic, A. Mester, J. Steinke, M. Weiss, S. Lewdeni-Schmid, T. Chaudhuri, and P. Stefanutti, "Power electronic traction transformer;medium voltage prototype," *Industrial Electronics, IEEE Transactions on*, vol. 61, no. 7, pp. 3257–3268, July 2014.

[9] X. She, S. Lukic, A. Huang, S. Bhattacharya, and M. Baran, "Performance evaluation of solid state transformer based microgrid in freedm systems," in *Applied Power Electronics Conference and Exposition (APEC), 2011 Twenty-Sixth Annual IEEE*, March 2011, pp. 182–188.

[10] H. Fan and H. Li, "High-frequency transformer isolated bidirectional dc-dc converter modules with high efficiency over wide load range for 20 kva solid-state transformer," *Power Electronics, IEEE Transactions on*, vol. 26, no. 12, pp. 3599–3608, Dec 2011.

[11] B. Zhao, Q. Song, and W. Liu, "A practical solution of high-frequency-link bidirectional solid-state transformer based on advanced components in hybrid microgrid," *Industrial Electronics, IEEE Transactions on*, vol. 62, no. 7, pp. 4587–4597, July 2015.

[12] H. Tao, J. Duarte, and M. Hendrix, "Three-port triple-half-bridge bidirectional converter with zero-voltage switching," *IEEE Transactions on Power Electronics*, vol. 23, no. 2, pp. 782–792, March 2008.

[13] S. Falcones, R. Ayyanar, and X. Mao, "A dc-dc multiport-converter-based solid-state transformer integrating distributed generation and storage," *IEEE Transactions on Power Electronics*, vol. 28, no. 5, pp. 2192–2203, May 2013.

[14] L. F. Costa, G. Buticchi, and M. Liserre, "Quad-active-bridge as cross-link for medium voltage modular inverters," in *IEEE Energy Conversion Congress and Exposition (ECCE)*, Sept 2015, pp. 645–652.

[15] R. De Doncker, D. Divan, and M. Kheraluwala, "A three-phase soft-switched high-power-density dc/dc converter for high-power applications," *IEEE Transactions on Industry Applications*, vol. 27, no. 1, pp. 63–73, Jan 1991.

[16] N. Schibli, "Symmetrical multilevel converters with two quadrant dc-dc feeding," Ph.D. dissertation, Swiss Federal Institute of Technology, 2000.